Chapter 15

Subcellular Optical Nanosurgery of Chromosomes

Linda Shi,[a] Veronica Gomez-Godinez,[c] Norman Baker,[b] and Michael W. Berns[a,c]

[a] *Institute of Engineering in Medicine and Department of Bioengineering, University of California, CA, USA*
[b] *Department of Electrical and Computer Engineering, University of California, San Diego, La Jolla, CA 92093, USA*
[c] *Beckman Laser Institute and Department of Biomedical Engineering, University of California, Irvine, CA 92697, USA*
zhixiashi@gmail.com

We describe two laser microirradiation optical platforms to study: (i) DNA damage responses following selective damage to a single mitotic chromosome arm and (ii) inhibition of cytokinesis resulting from damage to single and/or multiple chromosome tips (presumptive telomeres) of cells in the anaphase stage of mitosis. For studies on DNA damage a 200 femtosecond near-IR laser and a 12 nanosecond 532 nm second harmonic Nd:YVO_4 laser were used, and for microirradiation of chromosome tips a 532 nm 12 picosecond second harmonic Nd:YAG laser was used. The DNA damage studies showed that the structure of the alteration was the same for both lasers, and very specific chemical sensing and repair pathways were activated in mitosis. This was evidenced by the accumulation of these proteins at the irradiation sites. Irradiation of the chromosome

Understanding Biophotonics: Fundamentals, Advances, and Applications
Edited by Kevin K. Tsia

ISBN 978-981-4411-77-6 (Hardcover), 978-981-4411-78-3 (eBook)
www.panstanford.com

tips resulted in an inhibition or delay in cytokinesis in a significant percentage of cells. This result suggests that the chromosome tip, the location of telomere, may have a regulatory role in the final stage of cell division.

15.1 Introduction

This chapter will focus on recent studies that use microscope-focused laser light to alter submicrometer regions of chromosomes in living cells. The ability to use a focused laser to alter and/or ablate a submicron region of a pre-selected single chromosome [3, 5] or numerous other cell organelles [6, 7] has been the subject of many research articles, reviews, and three books [4, 8, 15, 25].

The fundamental physics of the ablation process is not well understood in single cell biological systems. It can be due to a linear absorption process such as heating or photochemistry, or it could be due to a non-linear process resulting in a micro-plasma, including shock waves, cavitation bubbles, and high electric fields. Or the ablation process may involve a combination of linear and non-linear processes [10]. Though there are good reviews on the subject [24], the physics of the ablation process of an organelle or structure inside a single living cell is not well characterized. Despite the lack of a precise understanding of the physics of subcellular ablation, laser micro- and nanosurgery have been used to alter and study virtually every cell organelle that can be visually resolved with the light microscope. This includes fluorescence using standard fluorophores or genetically expressed fusion proteins, the latter providing the ability to visualize and ablate structures such as a single microtubule. With a 25 nm diameter, a microtubule is well below the resolution of the optical microscope, yet it can be easily cut with a focused laser beam [11, 23].

In this chapter we describe two laser microirradiation optical platforms to study: (i) DNA repair following selective damage to a single mitotic chromosome arm and (ii) inhibition of cytokinesis resulting from damage to single and/or multiple chromosome tips (presumptive telomeres) of cells in the anaphase stage of mitosis.

15.2 Robotic Laser Microscope Systems Design

We have developed several robotic laser microscope systems with remote operational capabilities [10]. Each system is comprised of four key component systems: (i) the microscope and associated imaging systems, (ii) the laser sources, (iii) the array of controlling optical elements, and (iv) the computers and software–hardware interfaces. Here we mainly describe a single laser ablation system using two different laser sources.

15.2.1 *Robotic Laser Microscope Using a Picosecond Green Laser (RoboLase II)*

RoboLase II is comprised of an inverted microscope (Zeiss Axiovert 200M, Germany), external optics to direct the laser beam into the microscope, a CCD digital camera, and hardware-software for control of laser power, specimen stage and microscope stand focus and illumination. The optical setup is shown in Fig. 15.1 and the hardware block diagram is shown in Fig. 15.2. For ablation experiments, either a 40× oil NA 1.3 or 63 × 1.4 plan-apochromat PH3 oil objective is used. Optics external to the microscope guide the lasers into the microscope and provide automated laser power

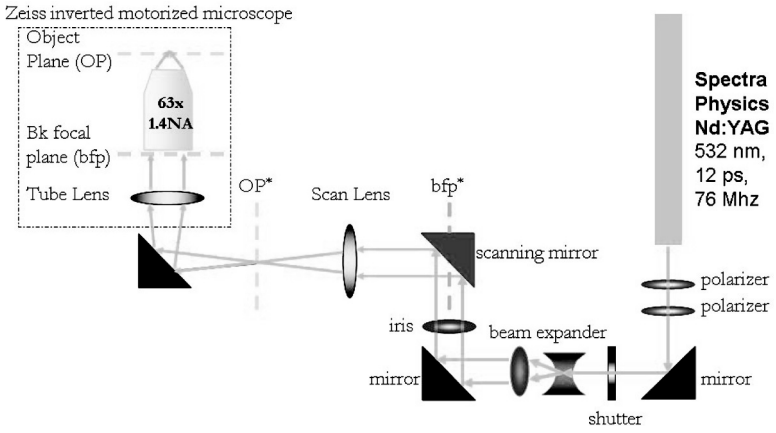

Figure 15.1 Optical design of RoboLase II.

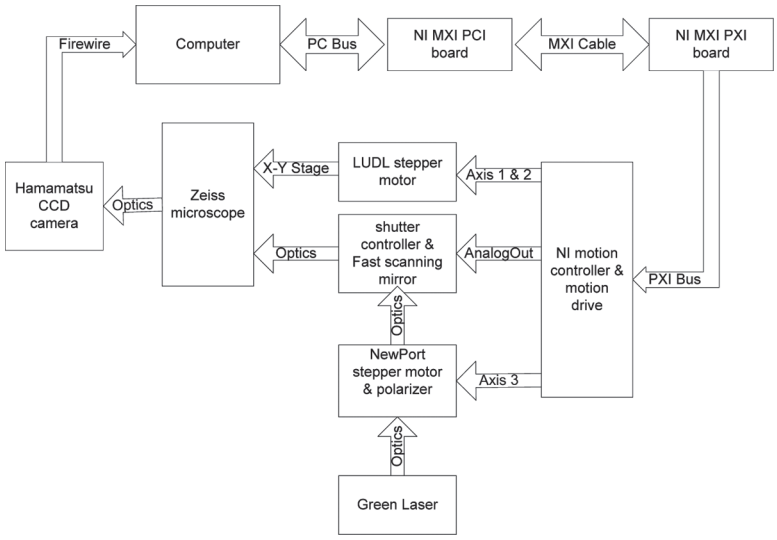

Figure 15.2 Hardware block diagram of RoboLase II.

control, laser shuttering, and laser power monitoring. The ablation laser is a diode-pumped Spectra-Physics Vanguard Nd:YAG with a second harmonic generator (SHG) providing a TEM00 mode 532 nm laser beam that is linearly polarized with 100:1 purity. The laser head emits 12 ps pulses at 76 MHz with a 2 W average power. The laser beam is transmitted through the first of two stationary glan polarizers (CLPA-12.0-425-675, CVI laser, LLC, Albuquerque, NM) in front of the laser cavity. The laser power is controlled by rotating the second polarizer mounted in a motorized rotational mount driven by an open-loop two-phase stepper motor with a 0.05 degree accuracy (PR50PP, Newport Corp, Irvine, CA). The stepper motor rotates the polarizer from its vertical orientation with maximum transmission to its horizontal orientation with minimum transmission well below the required threshold for ablation of cell organelles such as microtubules or chromosomes. The stepper motor is controlled via the flexmotion board in the PXI chassis. A mechanical shutter (Vincent Associates, Rochester, NY) gates the main laser beam to provide "short" (in our studies 30 ms duty cycle) bursts of macro-pulses to the microscope. The laser

beam is then expanded using an adjustable-beam expander (2-8×, 633/780/803 nm correction, Rodenstock, Germany) and lowered to a height just above the optical table by two additional mirrors. Telecentric beam steering is achieved by placing a single dual-axis fast scanning mirror (Newport Corp.) at an image plane conjugate to the back focal plane of the microscope objective. This image plane is formed by a 250 mm biconvex lens positioned with its front focal plane at the image plane of the under the microscope *Keller–Berns* port and with its back focal plane at the fast scanning mirror surface. To access the *Keller–Berns* port, the microscope is raised 70 mm above the table via custom-machined metal alloy posts to leave room for a 45 degree mirror, which vertically redirects incident laser light running parallel to the table. Once inside the microscope, the laser light passes through the tube lens and through an empty slot of the reflector turret before entering the back of the objective lens. All external mirrors in the ablation laser light path are virtually loss-less dielectric mirrors optimized for 45 degree reflections of 532 nm S-polarized light (Y2-1025-45-S, CVI Laser LLC). The fluorescence filter wheel contains filter cubes (Chroma Technology Corp., Bellows Falls, VT) that span the range for most commonly used fluorophores. The cubes are removable and can have excitation/absorption/bandpass filter combinations designed for any chromophore that a collaborator might use.

Specimens are mounted in an X-Y stepper stage (Ludl Electronic Products, Hawthrone, NY) controlled with a PXI-7344 stepper motor controller (National Instruments, Austin, TX) and an MID-7604 power drive (National Instruments). The motion board is mounted in a PXI chassis (National Instruments), connected to the host computer through two MXI4 boards (one in the PXI chassis, the other in the host computer) through the MXI-3 fiber-optic cable (National Instruments).

A high quantum efficiency digital camera is used to capture transmitted and fluorescent images. RoboLase implements a Hamamatsu ORCA-AG deep-cooled 1,344 X 1,024 pixel 12-bit digital CCD camera with digital (firewire) output. The ORCA can read out sub regions of the chip for increased frame rates, bin pixels for increased signal to noise, and adjust gain and exposure time to trade off between signal to noise characteristics and arc lamp exposure times.

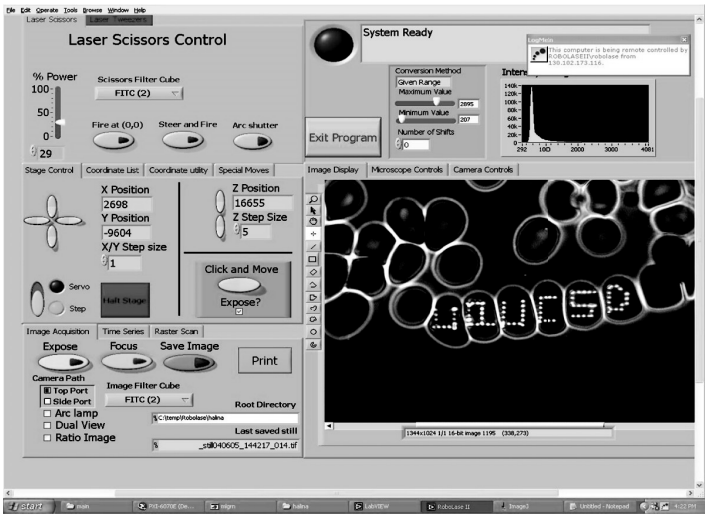

Figure 15.3 Front panel of RoboLase II.

The control software for this system is programmed in the LabVIEW (National Instruments) language and is responsible for control of the microscope, cameras, laser ablation and external light paths. The control software also manages image and measurement file storage. It communicates with the user through the graphic user interface or the "front panel" in LabVIEW. The front panel receives user input and displays images and measurements. The control software interprets commands sent by the user into appropriate hardware calls and returns the results of that action to the front panel and/or computer's hard drive. Emphasis is placed on the design of the front panel, such that it is easy to learn while providing the features needed to search for a cell of interest and then to perform cellular manipulation on that cell. Figure 15.3 shows an image of the front panel of RoboLase II.

15.2.2 *Robotic Laser Microscope with a Femtosecond Near-Infrared (NIR) Laser*

This laser system is built around a Ti:sapphire femtosecond near infrared (NIR) laser (Fig. 15.4). The NIR Ti:sapphire laser is a 76 MHz

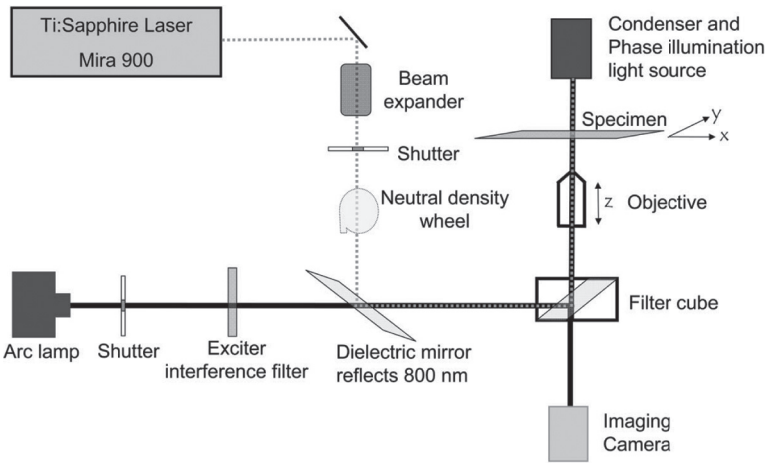

Figure 15.4 Optical design of RoboLase with femtosecond IR laser system [14].

~200 fs beam tunable between 720 and 850 nm (Coherent Mira Model Coherent Inc., Santa Clara, CA). The beam is coupled to the side port of a Zeiss inverted microscope (Axiovert 200M) via use of a series of highly reflective coated mirrors. A single dual-axis fast scanning mirror (Newport Corp.) in the beam path enables precise scanning of the beam in the microscope optical field. The beam is focused via a 63× (1.4 NA) microscope objective to a diffraction-limited spot. For 800 nm, the transmission factor of the Zeiss Plan-Apochromat 63× /1.4 NA objective was determined to be 0.6, using the dual objective method [14]. The pulse energy at the focused spot is varied by a control on the orientation of a Glan-Thompson polarizer mounted on a motorized rotational stage in the beam path. The scanning mirror is controlled by in-house developed software on a LabView platform to create a pattern of any desired geometry in the target cell or organelle. The macropulse exposure time (usually 20–30 milliseconds) of the focused spot is controlled by use of a computer-controlled mechanical shutter (Uniblitz). Since the laser is generating 200 femtosecond pulses at a rate of 76 MHZ, the total number of short micropulses exposing the target is considerable. A Hamamatsu ORCA-AG digital CCD camera with digital (firewire) output is used to capture transmitted and fluorescent images.

The system uses Labview to communicate and control the ORCA camera controller. Software for computer control of all hardware and image acquisition is similar to that described in the previous section.

15.3 Chromosome Studies

15.3.1 *DNA Damage Responses of Mitotic Chromosomes*

The natural occurrence of DNA damage within cells through endogenous metabolic by-products, DNA replication errors and environmental factors such as the sun's harmful UV rays has resulted in organisms evolving the ability to recognize and repair DNA damage. Unrepaired DNA damage can lead to an accumulation of mutations that can be deleterious to tissues through cell senescence, apoptosis or even up-regulated cell divisions. Understanding the responses to DNA damage is critical to understanding aging, developmental defects, and diseases such as cancer. The induction of DNA damage in a specified sub-micron linear region of interphase nuclei using microscope-focused laser beams is becoming a standard method to study cellular responses to DNA damage [9, 13, 16, 25]. However, only a few of these studies have looked at the DNA damage response in mitotic cells [1, 12, 19]. This is primarily due to the inherent difficulties associated with the rounding and eventual detachment of mitotic cells from their growing substrates. The fact that marsupial Ptk2 cells (*Potorous tridactylus)* remain very flat and adhere to the growing surface during mitosis, and that they have only 12 chromosomes, facilitates selective laser targeting [17].

Our recent studies have focused on two aspects of laser induced DNA damage/response in mitotic cells: (i) ultrastructural transmission electron microscope (TEM) characterization of the chromatin alteration produced either by the femtosecond near-IR (NIR), or the nanosecond green lasers, and (ii) immunostaining for the double stand break marker (γH2AX) as well as other proteins associated with (a) sensing of double strand breaks (DSBs) such as Nbs1 and Rad50 and (b) the actual repair of the damaged DNA, by the protein Ku.

Chromosomes observed 1–10 seconds post laser by phase contrast microscopy initially demonstrate paling (a change in refractive index) at the irradiation site (Fig. 15.5a,d). To examine the ultrastructural nature of this change, chromosomes in live cells were exposed to either the femtosecond near-IR (Fig. 15.5a–c)

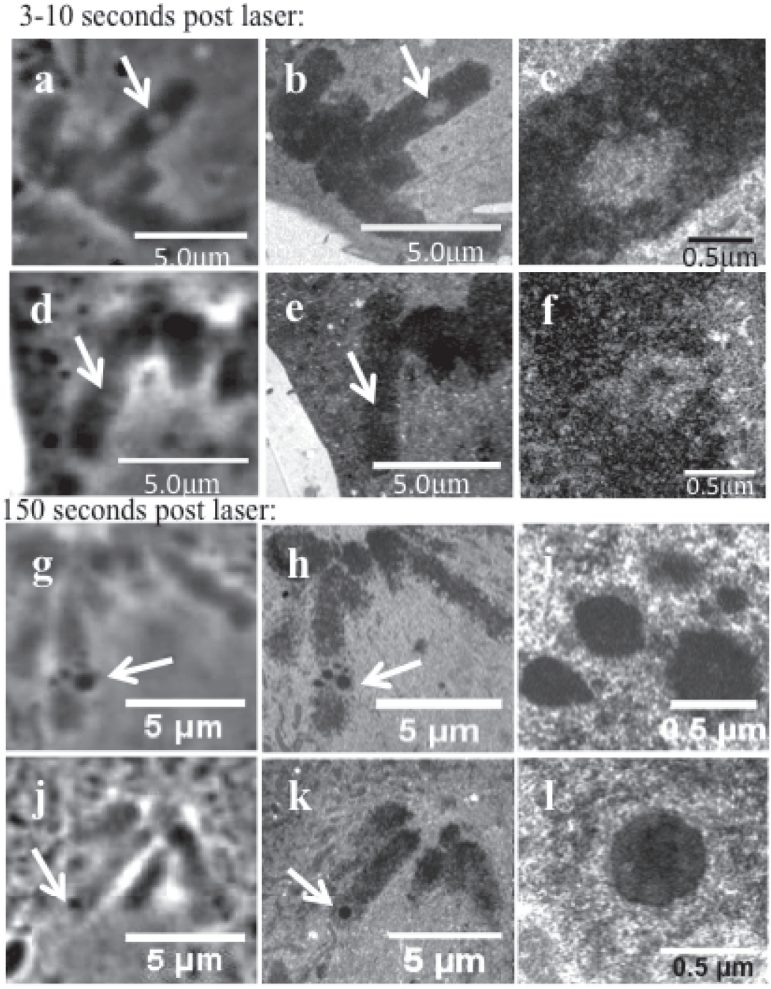

Figure 15.5 Phase (a, d, g, j) and transmission electron micrographs of cells damaged by the femtosecond near-IR (a–c and g–j) and nanosecond lasers (d–f and j–l) [14].

or nanosecond green lasers (Fig. 15.5d–f). They were fixed for TEM 3–10 seconds post laser, serial thin-sectioned, and examined using established TEM procedures. A phase image of an anaphase chromosome (Fig. 15.5a, arrow) shows the paling observed 3 seconds after laser exposure. Low and high magnification electron micrographs of the paled region demonstrate reduced electron density in that region (Fig. 15.5b,c). The diameter and shape of the paled area observed by phase contrast light microscopy is virtually the same as the TEM region showing diminished electron density. The diameter of the paled area in Fig. 15.5a is 0.8 μm, and in the corresponding electron micrograph it is 0.87 μm. An anaphase chromosome damaged by the green nanosecond laser also causes phase paling at the laser irradiation site (Fig. 15.5d, arrow). The corresponding low- and high-magnification electron micrographs (Fig. 15.5e,f) similarly reveal reduction in electron density corresponding to the phase paled region. The diameter of the light microscope phase paling is 0.7 μm (Fig. 15.5d) and for the TEM electron diminished zone it is 0.72 μm (Fig. 15.5e,f). Therefore, it is concluded that the chromosome alterations created by the femtosecond NIR and nanosecond green lasers are similar at the energy and power densities used in these studies: (i) phase-lightened (paled) regions when observed using phase contrast microscopy, and (ii) a diminution of electron density in the same region when observed by TEM [14].

Analysis of the changes occurring in the irradiation sites using immunostaining reveal that both lasers are capable of inducing a DNA DSB response (Fig. 15.6). This is evidenced by positive staining for the DSB marker γH2AX as well as the accumulation of proteins involved in DSB sensing, such as Nbs1 and Rad50. Fig. 15.6h shows a phase image of an anaphase chromosome fixed eight minutes post laser. Immunostaining for Nbs1 (Fig. 15.6j) shows strong fluorescence that appears to co-localize with the dark material when both images are overlapped (Fig. 15.6h). Figure 15.6k demonstrates fluorescence for γH2AX which extends beyond the actual lesion area. However, this is expected as γH2AX is known to spread beyond the damage site resulting in an amplification of the DSB signal [20]. Overlapping the γH2AX fluorescence image with the Nbs1 fluorescence image (Fig. 15.6n) and the phase dark

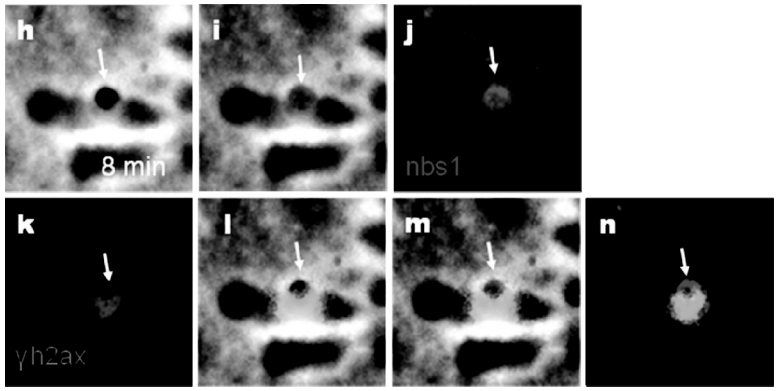

Figure 15.6 The femtosecond and near-IR lasers elicit a double strand break response as demonstrated by yH2AX and Nbs1 immuno-staining. Dark material is observed to co-localize with Nbs1. (h) An anaphase chromosome fixed eight minutes post laser. An arrow depicts the dark material that formed after laser irradiation. (i) Overlay between (j), Nbs1 fluorescence and (h). (j) Nbs1 fluorescence image. (k) γH2AX fluorescence image. (l) Overlay between (h) and (k). (m) Overlap of Nbs1 and γH2AX fluorescence with phase image. (n) Nbs1 and γH2AX fluorescence [14].

material (Fig. 15.6l) demonstrates that γH2AX does not co-localize with either Nbs1 or the phase dark material. Similar results were obtained when the green nanosecond laser was used [14].

To determine whether the DSB response in mitosis involves activation of a repair pathway in addition to DSB sensing, cells were immunostained for Ku (Fig. 15.7b), a heterodimer that is part of the non-homologues end joining (NHEJ) repair pathway. The results show co-localization between Ku and the phase dark material when metaphase cells are fixed and stained three minutes post laser (Fig. 15.7e). These results demonstrate that the near-IR and green nanosecond lasers can be used to elicit a DSB response which results in accumulation of a repair pathway protein in mitotic cells.

The formation of the dark material was identified to be a result of the accumulation of DNA damage response proteins as demonstrated by GFP-Nbs1 accumulation and immunostaining for Nbs1, Rad50, and Ku [14, 18]. The accumulation of the fluorescent fusion protein GFP-Nbs1 to mitotic chromosomes occurred in a

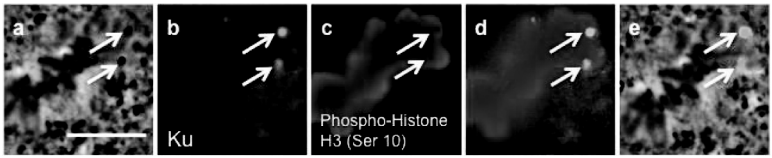

Figure 15.7 Ku, a heterodimer from the non-homologous end joining pathway, can recruit to mitotic chromosomes damaged by the laser. This example is from chromosomes damaged with the near-IR laser; however, the green can elicit the same response. Staining for a mitotic marker, histone H3 phosphorylated on Ser 10, demonstrates a lack of histone protein at the damaged area [14].

similar manner as the formation of the dark material. It increased in diameter and intensity over time. Further, visualization of Nbs1 through immunofluorescence was not observed prior to the formation of dark material. The co-localization of Nbs1 and Ku to the phase dark material supports the TEM observations that the dark material is an aggregation of electron dense material.

In addition to following chromosomes within mitosis, cells with laser-induced mitotic chromosome alterations have been followed into G1 [14]. The phase dark material persists into G1 and there is positive immunostaining for Nbs1 and Ku associated with this material. This result suggests that at least some of the DNA damage produced in mitosis is still being sensed, and repaired in G1 [14].

In summary, the studies reviewed here demonstrate that both the femtosecond near-IR and nanosecond green lasers are capable of creating damage that is in the submicron range which initially appears as a change in phase contrast (phase paling) and is subsequently characterized by the formation of phase dense dark material with a distinct ultrastructural character suggestive of accumulation of material. Fluorescence immunostaining of the irradiated region reveals DNA DSB response proteins, NBS1 and γH2AX, as well as the homologous end joining repair pathway protein Ku. The laser-induced damage produced on mitotic chromosomes was found to persist into G1 where γH2AX, Nbs1, and Ku continued to be associated with the phase dark material initiated in mitosis [14].

15.3.2 *Chromosome Tips (Telomeres) Regulate Cytokinesis*

Genome maintenance is crucial to survival of species and the maintenance of healthy tissues and organs throughout life. Lesions in DNA and subsequent repair pathways have been intensively studied, particularly in G1, S, and G2 [21]. As seen in the previous section, DNA damage response mechanisms during mitosis have only recently been studied [14].

Most of the DNA damage response studies in mitosis have focused on the period of before anaphase onset, prior to the chromosomes initialing movement to respective poles. In those studies, coupling DNA damage and repair to the spindle assembly checkpoint has been suggested [19], however it is not absolutely clear whether these mechanisms are actually related to the sensing of DNA damage [22].

In our recent studies we have continued to use PTK cells because they remain flat during cell division, and they have a relatively small number of large chromosomes (12) whereas most other cell types round-up during mitosis, and the chromosome numbers are generally much larger. Because of the large size and small number of chromosomes, these cells have been used in a significant number of studies employing laser-mediated damage [4, 5].

To investigate the response to DNA damage in mitosis after anaphase is initiated (separation of chromosomes) laser energy from the green picosecond RoboLase II system (see Section 15.2.1, Fig. 15.1) was applied to the chromosome arms, chromosome tips, or cytoplasm (Fig. 15.8A–C respectively) to evaluate the effects of disrupting these structures on progression through mitosis [2].

Laser ablation of the cytoplasmic region distal from the midzone resulted in no discernable morphological changes (Fig. 15.8C). Targeting of chromosome arms resulted in either a severing of the arm and production of a chromatin fragment free from the motion of the chromosome body (Fig. 15.8A), or an optical phase-contrast "paling" (i.e., change in refractive index) in the irradiated region of the chromosome without distinct severing of the chromosome arm was observed (see Fig. 15.8A,D in the previous section). Irradiation of the chromosome tips result loss of chromosome tip structure,

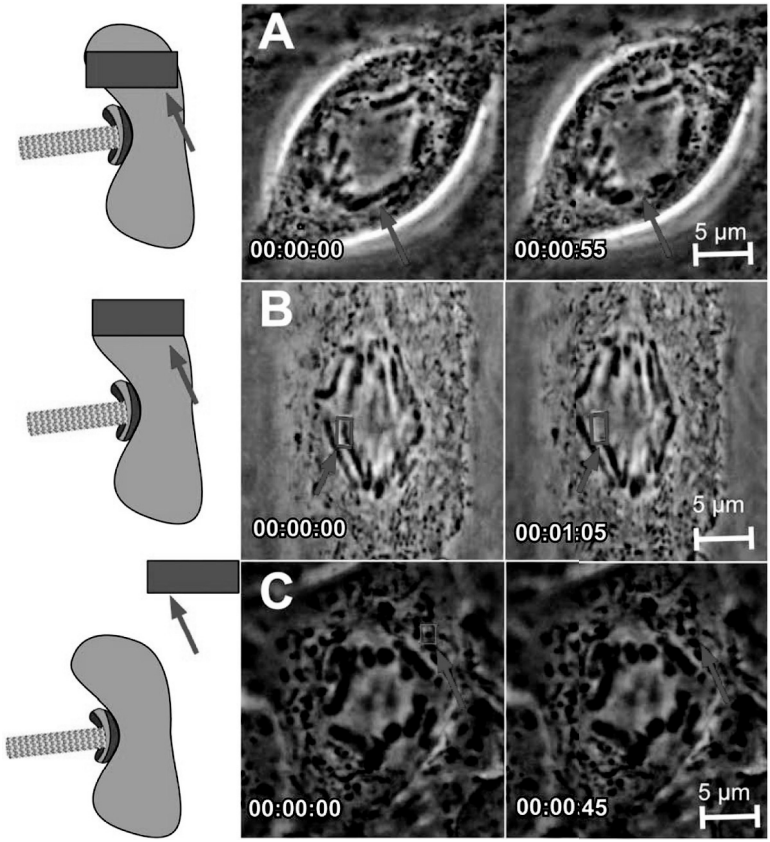

Figure 15.8 Examples of chromosome and cytoplasmic ablations. Left side is a cartoon of different irradiation sites (non-tip and tip chromosome ablation and non-chromosome -cytoplasm) ablation. (A) Arm chromosome ablation in the mid-region between chromosome tip and centromere preserving the distal remnant of the chromosome. (B) Chromosome tip ablation eliminates the distal region of the chromosome with no observable chromosome fragment remaining. (C) Cytoplasmic ablation avoids chromosomes but may be targeted within or outside the mitotic spindle [2].

also indicated by a distinct phase-lightening at the irradiation site (Fig. 15.8B).

Different effects were observed on the progression of anaphase depending on the location of the laser damage (see Table 15.1).

Table 15.1 Timing of mitotic exit for anaphase laser ablation to cytoplasm, chromosome arm and chromosome tips [2]

Region of ablation	Outcome	*n*	% total	Mean time (min)	STDEV
Cytoplasm distal to midzone	Cell divides	38	100	24	4
Cytoplasm midzone	Cell divides	33	100	49	11
Chromosome (non-tip)	Cell divides	76	100	26	7
Chromosome tip (single)	No furrow	16	16		
	Furrow regression	12	12	88	25
	Delay in division	39	40	70	15
	Cell divides	32	32	27	5
	Total cells	99			
Chromosome tip (multiple)	No furrow	32	37		
	Furrow regression	16	19	101	32
	Delay in division	21	24	79	14
	Cell divides	17	20	30	4
	Total cells	86			

In cells with selective focal laser damage to non-tips of the chromosomes (non-telomere regions) normal timing of cell division including completion of cytokinesis was observed ($N = 95$) (Fig. 15.9b). However, targeting of one chromosome tip resulted in 68% of cells with disrupted mitotic progression. Only 32% of the tip-irradiated cells underwent cytokinesis similar to control non-tip-abated cells. The remainder of tip-irradiated cells were divided into three categories: (1) cells that did not initiate a furrow after more than two hours post-irradiation (16%), (2) cells that had furrow regression after initiating cytokinesis (12%), or (3) cells with delayed furrow formation followed by cytokinesis (30%).

Chromosome tip ablation also impacted the duration of cell division (Fig. 15.9A). While $>$90% of control cells including non-irradiated and cells subjected to cytoplasmic ablation distal from the midzone or chromosome arms completed cytokinesis within 30 minutes, 68% of cells in which chromosome tips were ablated did not complete cytokinesis within this time frame. Of the cells that were delayed, approximately half exhibited an extended delay, particularly in the earliest stages of furrow initiation (Fig. 15.9B, blue). These observations indicate that, unlike damage to a

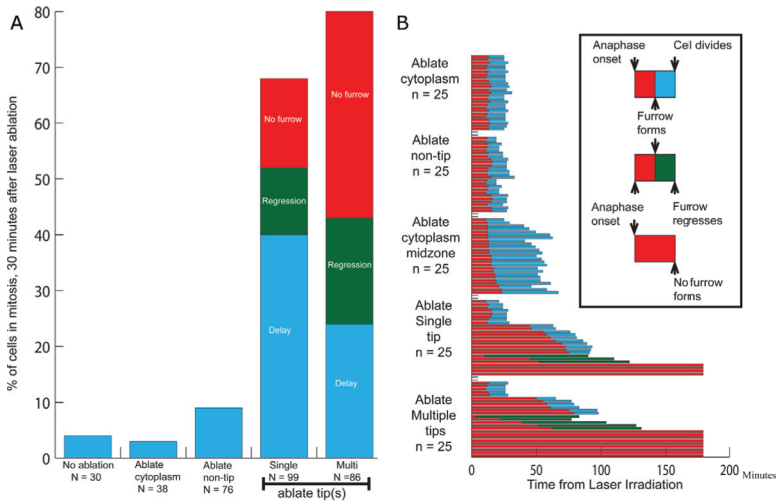

Figure 15.9 (A) Chromosome tip ablation delays exit from mitosis. Control mitotic cells or cytoplasm and arm laser ablation treated cells predominantly exit mitosis within 30 minutes of anaphase onset. However, single or multiple chromosome tip ablations result in a dramatic increase in delayed mitotic exit (red, no furrow formed; green, furrow regression; and blue, normal cytokinesis exit). (B) Timeline for control and chromosome tip ablation. Time histograms of 25 representative cells each for cytoplasmic ablation distal from the midzone, chromosome arm ablation, cytoplasmic midzone ablation, and single and multiple chromosome tip ablation. The inset-rectangle on the right side of the figure defines the transitions as well as the beginning and end-points of the cell data in the figure. Transitions are based on morphological criteria of anaphase onset, furrow formation, furrow regression and successful cell division [2].

chromosome arm, damage to the tip, the presumptive telomere, negatively impacts progression through cytokinesis.

To examine whether there is a quantitative relationship between the number of tips (telomeres) damaged and the inhibition of cytokinesis, experiments were conducted in which more than one tip was irradiated. In these experiments 56% of the cells subjected to multiple (two or three) tip ablations (Table 15.1) either did not form a furrow or had furrow regression after it was formed. Since this is more than a two-fold increase compared to single tip ablation, the results demonstrate that multiple tip ablations increase

the proportion of cells with disrupted cytokinesis. Notwithstanding, this increase of cytokinetic defects could be due to inaccuracy in laser targeting, whereas multiple laser exposures increases the probability of successfully hitting a tip. On the other hand, multiple tip ablations may result in a cumulative effect, resulting in an increase in the frequency of cytokinesis defects.

In summary, the results of laser tip ablation implicate telomeres as regulatory sites for cytokinesis and suggest a telomere-based signaling pathway that couples post-segregation chromosome damage to completion of cell division. This pathway is possibly linked to DNA repair; however, the existence of other telomeric-specific protein damage/repair pathways cannot be excluded.

15.4 Conclusions

This review has focused on the genetic-bearing structure, the chromosome, because it has been studied more than any other cell structure using laser microirradiation. Recent advances in understanding DNA damage and repair have been possible using this approach and will likely expand in the future. In addition, the studies on ablation of chromosome tips are particularly relevant in light of the recent high interest in the function of telomeres and their relation to both ageing and oncogenesis. Finally, for the bioengineer and the biologist, we have shown that laser nanosurgery is not necessarily laser-specific. In other words, with carefully chosen irradiation parameters, such as wavelength, pulse duration, and energy delivery, similar biological and structural effects can be produced. However, it is important for all investigators to provide details on the exact lasers and irradiation parameters used so that studies can be clearly understood, compared, and replicated.

Acknowledgements

The authors would like particularly to thank Kyoko Yokomori, Jagesh Shah, and Samantha Zeitlin for their contributions to the original work described in this review. They provided key insight and

support for those studies. We also acknowledge the Beckman laser Institute Foundation for the financial support to conduct much of this work.

References

1. Anantha, R., Sokolova, E., and Borowiec, J. (2008). RPA phosphorylation facilitates mitotic exit in response to mitotic DNA damage, *Proc. Natl. Acad. Sci.,* **105**(35), pp. 12903–12908.
2. Baker, N. M., Zeitlin, S. G., Shi, L. Z., Shah, J., and Berns, M. W. (2010). Chromosome tips damaged in anaphase inhibit cytokinesis, *PLoS One*, **5**(8), pp. e12398.
3. Berns, M. W., Olson, R. S., and Rounds, D. E. (1969). *In vitro* production of chromosomal lesions using an argon laser microbeam, *Nature,* **221**, pp. 74–75.
4. Berns, M. W. (1974). *Biological Microirradiation*, Prentice Hall Series on Biological Techniques, Englewood Cliffs, USA.
5. Berns, M. W. (1974). Directed chromosome loss by laser microirradiation, *Science*, **186**, pp. 700–705.
6. Berns, M. W., Aist, J., Edwards, J., Strahs, K., Girton, J., McNeill, P., Rattner, J. B., Kitzes, M., Hammer-Wilson, M., Liaw, L. H., Siemens, A., Koonce, M., Peterson, S., Brenner, S., Burt, J., Walter, R., van Dyk, D., Coulombe, J., Cahill, T., and Berns, G. S. (1981). Laser microsurgery in cell and developmental biology, *Science*, **213**, pp. 505–513.
7. Berns, M. W., Wang, Z., Dunn, A., Wallace V., and Venugopalan, V. (2000). Gene inactivation by multiphoton-targeted photochemistry. *Proc. Natl. Acad. Sci.*, **97**, pp. 9504–9507.
8. Berns, M. W. (2007). A history of laser scissors (microbeams), *Laser Manipulation of Cells and Tissues*, ed. Berns, M. W., and Greulich, K. O., Academic Press, San Diego, Methods in Cell Biology, **82**, pp. 3–58.
9. Botchway, S. W., Reynolds, P., Parker, A. W., and O'Neill, P. (2010). Use of near infrared femtosecond lasers as sub-micron radiation microbeam for cell DNA damage and repair studies, *Mutat. Res*., **704**, pp. 38–44.
10. Botvinick, E. L., Berns, M. W. (2005). Internet-based robotic laser scissors and tweezers microscopy, *Microsc. Res. Tech.*, **68**(2), pp. 65–74.
11. Colombelli, J., Reynaud, E. G., Rietdorf, J., Pepperkok, R., and Stelzer, E. H. (2005). In vivo selective cytoskeleton dynamics quantification in

interphase cells induced by pulsed ultraviolet laser nanosurgery, *Traffic (Oxford, U.K.)* **6**(12), pp. 1093–1102.

12. Giunta, S., Belotserkovskaya, R., and Jackson, S. P. (2010). DNA damage signaling in response to double-strand breaks during mitosis, *J. Cell Biol*., **190**(2), pp. 197–207.
13. Gomez-Godinez, V., Wakida, N. M., Dvornikov, A. S., Yokomori, K., Berns, M. W. (2007). Recruitment of DNA damage recognition and repair pathway proteins following near-IR femtosecond laser irradiation of cells, *J. Biomed. Opt.,* **12**(2), 020505.
14. Gomez-Godinez, V., Wu, T., Sherman, A. J., Lee, C. S., Liaw, L. H., Zhongsheng, Y., Yokomori, K., and Berns, M. W. (2010). Analysis of DNA double-strand break response and chromatin structure in mitosis using laser microirradiation, *Nucleic Acids Res.,* **38**, e202.
15. Greulich, K. A. (1999). *Micromanipulation by Light in Biology and Medicine*, Birkhausr Verlag, Basel.
16. Kong, X., Mohanty, S. K., Stephens, J., Heale, J. T., Gomez-Godinez, V., Shi, L. Z., Kim, J. S., Yokomori, K., and Berns, M. W. (2009). Comparative analysis of different laser systems to study cellular responses to DNA damage in mammalian cells, *Nucleic Acids Res.*, **37**, e68.
17. Liang, H., and Berns, M. W. (1983). Establishment of nucleolar deficient sublines of PtK2 (Potorous tridactylis) by ultraviolet laser microirradiation, *Exp Cell Res.* **144**, pp. 234–240.
18. Mari, P. O., Florea, B. I., Persengiev, S. P., Verkaik, N. S., Bruggenwirth, M., Modesti, M., Giglia-Mari, G., Bezstarosti, K., Demmers, J. A., Luider, T. M., Houtsmuller, A. B., and van Gent, D. C. (2006). Dynamic assembly of end-joining complexes requires interaction between Ku70/80 and XRCC4, *Proc. Natl. Acad. Sci.*, **103**, pp. 18597–18602.
19. Mikhailov A., Cole R. W., Rieder, C. L. (2002). DNA damage during mitosis in human cells delays the metaphase/anaphase transition via the spindle-assembly checkpoint, *Curr. Biol.*, **12**, pp. 1797–1806.
20. Rogakou, E. P., Boon, C., Redon, C., and Bonner, W. M. (1999). Megabase chromatin domains involved in DNA double-strand breaks in vivo, *J. Cell Biol.*, **146**, pp. 905–916.
21. Shrivastav, N., Li, D., and Essigmann, J. M. (2010). Chemical biology of mutagenesis and DNA repair: cellular responses to DNA alkylation. *Carcinogenesis,* **31**, pp. 59–70.
22. Skoufias, D., Lacroix, F., Andreassen, P., Wilson, L., and Margolis, R. (2004). Inhibition of DNA decatenation, but not DNA damage, arrests cells at metaphase, *Mol Cell*, **15**, pp. 977–990.

23. Wakida, N. M., Lee, C. S., Botvinick, E. L., Shi, L. Z., Dvornikov, A., and Berns, M. W. (2007). Laser nanosurgery of single microtubules reveals location dependent depolymerization rates, *J. Biomed. Opt.,* **12**, pp. 1–8.
24. Vogel, A., Noack, J., Huttman, G., and Paltauf, G. (2005). Mechanisms of femtosecond laser nanosurgery of cells and tissue, *Appl. Phys. B*, **81**(8), pp. 1015–1047.
25. Yokomori, K., and Berns, M. W. (2010). Analysis of DNA double-strand break response and chromatin structure in mitosis using laser microirradiation, *Nucleic Acids Res.,* **38**, e202.